Continuous Flow Atomic Force Microscopy Imaging Reveals Fluidity and Time-Dependent Interactions of Antimicrobial Dendrimer with Model Lipid Membranes

Tania Kjellerup Lind,[†,‡] Paulina Zielińska,[§] Hanna Pauliina Wacklin,[†,‡] Zofia Urbańczyk-Lipkowska,[§] and Marité Cárdenas[†,*]

[†]Nano-Science Center and Institute of Chemistry, Copenhagen University, København DK2100, Denmark, [‡]European Spallation Source ESS AB, 221 00 Lund, Sweden, and [§]Institute of Organic Chemistry, Polish Academy of Science, 01-224 Warszawa, Poland

ABSTRACT In this paper, an amphiphilic peptide dendrimer with potential applications against multi-resistant bacteria such as *Staphylococcus aureus* was synthesized and studied on model cell membranes. The combination of quartz crystal microbalance and atomic force microscopy imaging during continuous flow allowed for *in situ* monitoring of the very initial interaction processes and membrane transformations on longer time scales. We used three different membrane compositions of low and high melting temperature phospholipids to vary the membrane properties from a single fluid phase to a pure gel phase, while crossing the phase coexistence boundaries at room temperature. The interaction mechanism of the dendrimer was found to be time-dependent and to vary remarkably with the fluidity and coexistence of liquid—solid phases in the membrane. Spherical micelle-like dendrimer—lipid aggregates were formed in the fluid-phase bilayer and led to partial solubilization of the membrane, while in gel-phase membranes, the dendrimers caused areas of local depressions followed by redeposition of flexible lipid patches. Domain coexistence led to a sequence of events initiated by the formation of a ribbon-like network and followed by membrane solubilization *via* spherical aggregates from the edges of bilayer patches. Our results show that the dendrimer molecules were able to destroy the membrane integrity through different mechanisms depending on the lipid phase and morphology and shed light on their antimicrobial activity. These findings could have an impact on the efficacy of the dendrimers since lipid membranes in certain bacteria have transition temperatures very close to the host body temperature.

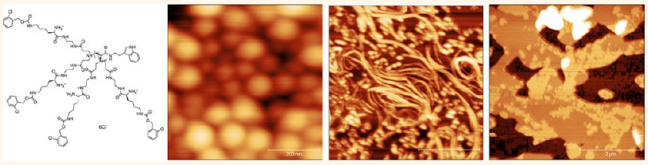

KEYWORDS: dendrimer · antimicrobial · AFM · QCM-D · lipid bilayers · membrane interactions

Ever increasing problems with bacteria growing resistant to common antibiotics have led to many outbreaks costing not only human lives[1] but also involving economic losses due to food recalls.[2] In order to combat fatal bacterial infections in the future, there is an urgent need for novel approaches that are less likely to induce resistance. Conventional antibiotics inhibit bacterial growth mainly by acting on specific protein targets and inhibiting central metabolic pathways.[3] This specific mechanism is effective but, combined with the overuse of antibiotics, it also increases the risk of resistance due to bacterial mutations and transfer of resistance genes.[4]

One of the answers to bacterial multiresistance is thought to be the development of new types of drugs, which act on microbes in a more nonspecific manner and thus are less susceptible to resistance-forming mechanisms. An attractive alternative is the use of synthetic analogues of natural antimicrobial peptides (AMPs), which are the first defense mechanism in the innate immune system of a wide variety of organisms.[5,6] Synthetic AMPs were originally engineered in linear forms[7] resembling their biological counterparts, but more recently, dendrimers based on a lysine backbone were synthetized.[8] The majority of AMPs are polycationic, amphipathic peptides enriched in hydrophobic and basic residues,

* Address correspondence to cardenas@nano.ku.dk.

Received for review August 30, 2013 and accepted December 4, 2013.

Published online December 04, 2013
10.1021/nn404530z

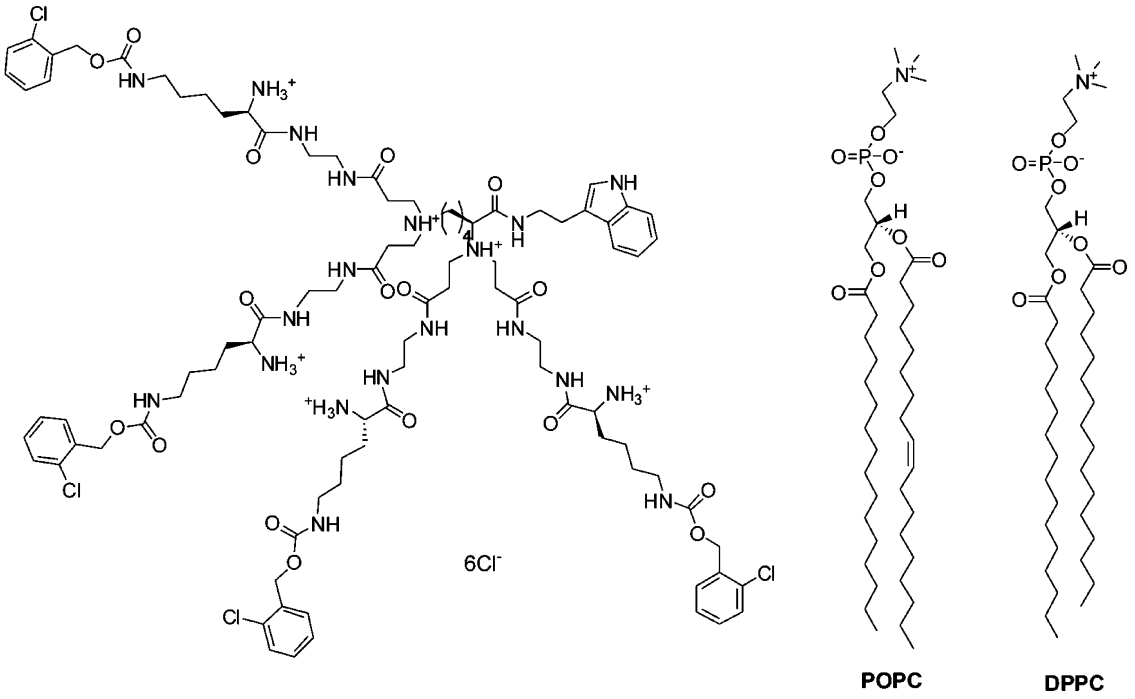

Figure 1. Chemical structures of amphiphilic branched analogue of lysine (BALY) hexachloride dendrimer and the two phospholipids, POPC and DPPC, used for formation of supported lipid bilayers in ratios giving rise to varying fluidity (0, 80, and 100 mol % DPPC).

and although highly diverse in sequence and secondary structure, they generally exhibit broad activity against microbes ranging from Gram-positive and Gram-negative bacteria over yeast, fungi, and viruses.[9,10]

Multiple charges are typically a prerequisite to antimicrobial activity, and thus polyvalent dendrimers carrying amino or ammonium groups, such as poly(amidoamine) (PAMAM),[11] poly(propyleneimine) (PPI),[12] or carbosilane[13,14] compounds are potent against common Gram-positive and Gram-negative bacteria. In order to enhance the biocidal activity and self-assembly at lipid interfaces, dendrimers can be rendered amphipathic by partial (statistical) substitution, for example, of the terminal amino groups in PAMAM dendrimers by polyethylene glycol groups[11] or introduction of a single/double aliphatic tail.[15] Also, amino-terminated antimicrobial peptide dendrimers showing selectivity toward negatively charged bacterial membranes have recently been identified by screening of a 6750-membered combinatorial library.[16,17] Here, we use low molecular weight peptide dendrimers assembled from basic (Lys, Arg) and lipophilic (Phe, Ala, Trp, *etc.*) amino acids that contain a balance between positively charged and lipophilic groups both in the dendrimer interior and at its surface.[18]

These novel dendritic amphiphiles exhibit significant potency against bacteria from Gram-positive and Gram-negative genera, including methicillin-resistant *Staphylococcus aureus* (MRSA) and extended spectrum β-lactamase (ESBL) variants[18−20] as well as antifungal activity against the *Candida albicans* genus. The activity and hemotoxicity of these cationic peptide dendrimers depend largely on the degree of branching as well as the distribution and types of functional groups present on the dendrimer surface.

Cationic antimicrobial peptides are generally thought to disrupt the structural integrity of bacterial membranes *via* initial electrostatic interactions with negatively charged lipids that are characteristic for these.[21] The following sequence of events is often hard to characterize at the molecular level, and several possible mechanisms have been proposed for peptides of different length, hydrophobicity, charge, and secondary structure.[9,22] The proposed mechanisms include pore formation, membrane solubilization, peptide translocation, and membrane thinning. All mechanisms described are believed to be initiated by surface association of the hydrophilic part of the peptide with the lipid headgroups, followed by membrane interruption at a threshold peptide concentration.[22,23] Although many studies have contributed to establishing the molecular mechanism of antimicrobial peptides in natural and model membranes, no experimental data on amphiphilic antimicrobial peptide dendrimers have been published to date. Given their great potential as bactericides and their structural differences from natural peptides and PAMAM dendrimers, there is thus a current need to relate particular mechanisms of antimicrobial activity to specific types of dendrimers.[24]

In order to understand the mechanism of action for amphiphilic antimicrobial dendrimers, we have

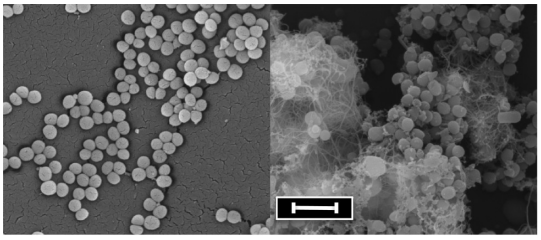

Figure 2. Scanning electron microscopy images of S. aureus ATCC 25923 cells prior to exposure (left) and after 8 h of incubation with BALY in 4 μM concentration (right). The scale bar is 2 μm and applies to both images.

undertaken systematic studies on the interaction between model phospholipid membranes and a branched analogue of lysine (BALY) dendrimer with the chemical formula $C_{92}H_{132}O_{17}N_{20}Cl_4 \times 6HCl$ (M_w = 2150.7 g/mol), the structure of which is shown in Figure 1. The analytical data and biological properties are described in the Materials and Methods, and organic synthesis is in the Supporting Information. BALY is an amphiphilic, flexible molecule having four long arms terminated in lipophilic 2-chlorocarbobenzoxy groups while carrying an indole moiety at the carboxy end. Like the majority of natural antimicrobial peptides, BALY is highly cationic, containing six positive charges, situated at the primary and ternary amine groups. Moreover, this structure has the potential to promote molecular self-assembly and dendrimer/membrane recognition *via* nonbonding intermolecular interactions such as classic and charge-assisted H-bonding, Cl···Cl, $\pi\cdots\pi$, van der Waals interactions, and most of all electrostatic forces. These chemical properties give rise to a very low minimal inhibitory concentration (MIC) of ~1 μM against Gram-positive *S. aureus* with cell lysis occurring at four-fold MIC (see Figure 2) and with 10-fold selectivity over Gram-negative *Escherichia coli* (see Table S1 in Supporting Information for MICs toward various bacterial strains).

To investigate the dendrimer−membrane interaction mechanism at the molecular level, we used single-lipid-supported membranes and binary mixtures of well-known high melting temperature (1,2-dipalmitoyl-*sn*-glycero-3-phosphocholine, DPPC) and low melting temperature (1-palmitoyl-2-oleoyl-*sn*-glycero-3-phosphocholine, POPC) zwitterionic lipids (see Figure 1 for representations of the chemical structures of the molecules used in this work). Three different compositions (0, 80, and 100 mol % of DPPC, in the following referred to as POPC, 80 mol % DPPC, and DPPC, respectively) were used to constitute our model cell membrane system since they produce supported lipid bilayers with physical properties (in terms of fluidity) close to native membranes[25−27] as well as coexisting gel- and fluid-phase domains. To detect structural changes during the dendrimer−membrane interaction, we applied two complementary surface-sensitive techniques: dissipation-enhanced quartz crystal microbalance (QCM-D) and atomic force microscopy (AFM) optimized for imaging under liquid flow conditions.

RESULTS

Dendrimer Adsorption on a Clean, Negatively Charged Surface. The adsorption behaviors of BALY on a clean silica surface and on lipid bilayers were assessed by QCM-D. QCM-D is an acoustic technique that measures mass adsorption/desorption at a surface in a controllable liquid environment. QCM-D records the changes in frequency (Δf) of an oscillating quartz crystal (related to mass changes) and the changes in dissipation of energy (Δd) in the adsorbed layer (related to viscosity and elasticity).[28] This is a widely used method for following interfacial processes *in situ* and has been used extensively for investigating lipid bilayer formation and their interactions with biomolecules.[29,30] In general, a decrease in Δf indicates mass adsorption, but more complex mechanisms can be revealed by also including the dissipation changes since these give information about the flexibility and the amount of coupled water in the system. A plot of Δd against Δf allows for an easy determination of whether the interaction mechanism is driven by pure adsorption/desorption (a horizontal, linear dependence) or involves several and more complex interactions.

Dendrimer adsorption to a clean silica surface was investigated using QCM-D in order to establish the adsorption behavior over a range of concentrations and for selecting an appropriate concentration to use for membrane experiments. After 1 h of dendrimer adsorption under flow and 1 h of equilibration, the sensor surfaces were rinsed in buffer for an additional hour. The resulting adsorption isotherms are shown in Figure 3A, where absolute changes in frequency after adsorption (blue) and after rinsing (black) are given as a function of concentration. Interestingly, a plateau at approximately −15 Hz in the adsorption isotherm was observed at low concentrations (1−10 μM), while higher concentrations led to excess dendrimer adsorption. This excess adsorbed amount could be rinsed away with buffer, leaving an irreversibly bound dendrimer layer corresponding to that formed at low concentrations. This suggests that at high concentrations the dendrimers self-aggregate at the surface, forming reversibly bound multilayers and that, after extensive rinsing, the final plateau corresponds to a monolayer of dendrimer molecules. This agrees with the dissipation data, which were negligible ($<0.5 \times 10^{-6}$) for concentrations below 15 μM and rose above 1×10^{-6} only at higher concentrations.

Using AFM, dendrimer adsorption on a clean mica surface could be observed by imaging in continuous flow mode, where the injected dendrimers reached the surface halfway through the scan, thus allowing for a direct monolayer thickness measurement from the zero height reference in the first half of the image

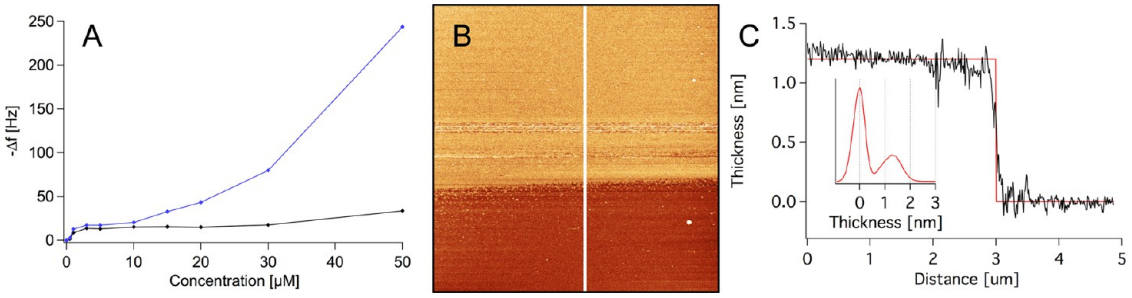

Figure 3. (A) Adsorption isotherm obtained from QCM-D experiments. Different concentrations of BALY were allowed to adsorb under constant flow for 1 h (blue curve) after which the pump was turned off for an additional hour before rinsing with PBS for 1 h (black curve). The *y*-axis gives the absolute change in frequency, which is directly proportional to the adsorbed mass in a nondissipative system. (B) AFM image of the initial adsorption and formation of a monolayer of BALY under liquid flow conditions. (C) Height profile (black) and fitted step function (red) across the image in B as indicated by the white line. Inset in C: height distribution function of B.

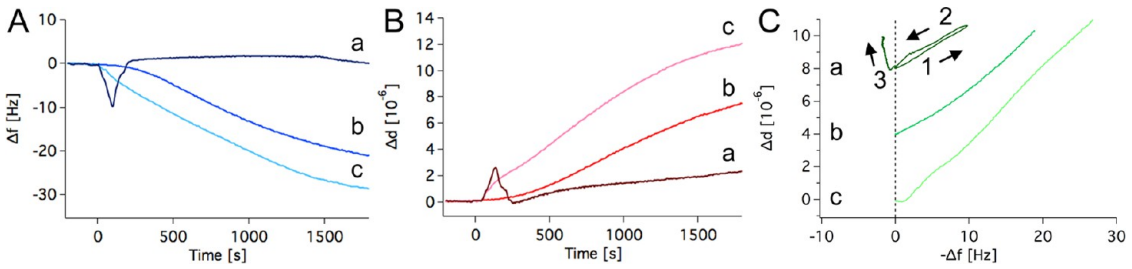

Figure 4. (A,B) Frequency (blue) and dissipation (red) changes for (a) POPC, (b) DPPC, and (c) 80 mol % DPPC membranes upon interaction with 6 μM dendrimer. Note that the curves have been offset to zero after membrane formation, and the changes are thus relative to the original membrane. (C) Curves of $\Delta d/-\Delta f$ for the three experiments. Note that all curves have been zeroed after membrane formation and offset by 4 Hz in the *y*-direction for clarity. The line going through zero thus indicates the reference values for the membrane before interaction ($\Delta f \approx -25$ Hz, $\Delta d < 1$). In (a), arrows and numbers 1−3 correspond to three distinct mechanisms; see text for a detailed account.

(Figure 3B,C). In this case, a 6 μM dendrimer solution was used because this corresponds to a plateau for monolayer formation (Figure 3A). Besides the dense monolayer, no further adsorption or surface aggregation was observed (Figure 3B), in agreement with the QCM-D data for this concentration. Once the complete layer was formed, it was not possible to distinguish it from the mica substrate due to its high coverage and low roughness, thus eliminating further attempts of thickness measurements after the first image. The thin dendrimer layer of 1.2 $\pm$ 0.1 nm suggests that the molecules flattened on the surface, due to favorable electrostatic interactions between positively charged amino groups on the dendrimer and the negatively charged mica surface.

Dendrimer Interaction with Lipid Bilayers As Followed by QCM-D. We decided to study the interaction of dendrimers with model membranes at concentrations at which they did not undergo multilayer formation. The initial interaction between 6 μM dendrimer and the three model lipid bilayers was investigated by QCM-D (for full set of overtones, see Supporting Information Figure S1). In the case of a fluid membrane, an initial fast decrease in frequency change (increase in mass) was observed, followed by a similar increase (decrease in mass) with opposite trend for the dissipation curve (curves indicated by (a) in Figure 4A,B, respectively). By plotting the change in dissipation as a function of the change in frequency, three distinct types of mechanisms could be resolved (#1−3 in Figure 4C). The first part of the curve was a straight line with positive slope (1) representing a mass increase, in agreement with an initial dendrimer adsorption process. The slope indicated that it was not a pure adsorption but a mass change involving layer softening, often interpreted as an increase in the amount of coupled water. This process was followed by a turn and a downward straight curve (2) with similar slope, indicating desorption to the same extent as the initial adsorption process. When this process reached $\Delta f = 0$, a new process (3) with a much steeper and negative slope appeared, meaning that the dissipation of the layer still increased, while the mass change converged. The signal furthermore experienced a significant spread of the overtones (Supporting Information Figure S1a), suggesting the formation of a softer, more dissipative layer. Altogether, the QCM-D data indicate a major rearrangement of the adsorbed layer.

For pure DPPC and for 80 mol % DPPC (Figure 4 curves b and c, respectively), the interaction pointed toward overall adsorption. QCM-D did not give indication of any desorption process for DPPC-containing membranes within the time of the measurement. However, desorption could have been masked due to

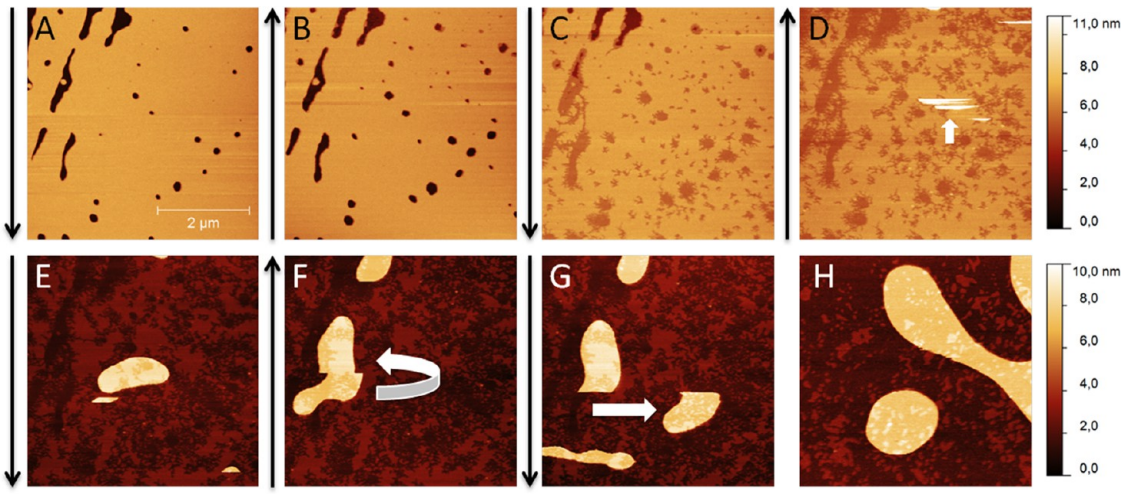

Figure 5. (A–G) Time-lapse series of AFM images of a gel-phase bilayer of DPPC captured under continuous flow of dendrimer at 1 μM concentration. The scale bar in A applies to all images, and the black arrows indicate the scan direction. Interaction steps include dendrimer adsorption, expansion of local depressions in a star-like channeling pattern, and redeposition of soft, flexible lipid patches; see text for a detailed account and Figure 6 for close-ups of the interaction steps. (H) Image captured on day 2 assures that no significant changes have occurred on a longer time scale.

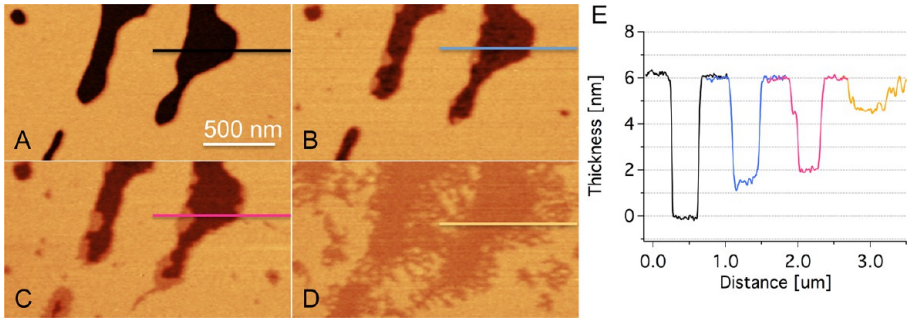

Figure 6. Close-ups of the initial stages of interaction between the dendrimer and DPPC. The scale bar in A applies to all images. (A) Image of the membrane prior to interaction with BALY. Note the new holes formed already in frame B due to interaction with dendrimers. (E) Graph showing color-coded height profiles corresponding to the lines given in A–D. Note that the curves have been shifted in the *x*-direction for clarity and thus represent a time evolution, meaning that the *x*-axis shows only relative distances.

a faster and stronger adsorption process in the averaged QCM-D signal. The slopes of the $\Delta d/-\Delta f$ curves were similar for POPC and DPPC at the initial stages, but for DPPC, the graph curved slightly and followed a power function instead of a straight line. A steeper slope was seen for the 80 mol % DPPC membrane, indicating a softer, more hydrated layer in this case. Also, a noticeable distinction between the three experiments was the initial lag time for the gel-phase membrane before a significant change could be observed. The QCM-D data were recorded over a period of 25 min and thus only give information about the initial steps of the dendrimer–membrane interaction.

AFM Imaging of Interaction with a Gel-Phase DPPC Bilayer. Due to the fluidity-dependent behaviors observed using QCM-D, AFM imaging was carried out for a visual interpretation. Figure 5 (and close-ups in Figure 6) shows consecutive AFM images of a DPPC bilayer under continuous flow of a 1 μM dendrimer solution. An area with defects was intentionally chosen as the starting frame (Figure 5A and Figure 6A), with the purpose of simultaneously investigating if the dendrimer had a preferential interaction with existing gaps and/or large patches of unbroken bilayer. From height analysis of the defects in the bilayer prior to dendrimer addition, the thickness could be determined to be 6.0 $\pm$ 0.2 nm, which is consistent with literature;[27] see Supporting Information Figure S2. In Figure 5B, the dendrimer flow was initiated while scanning the surface from the bottom up (as indicated by the black arrow). Thus, the dendrimer–membrane interaction was observed in the last half of the frame as the dendrimers reached the surface. Interestingly, height profiles spanning defects in the bilayer revealed that dendrimers first adsorbed to the bare mica (Figure 6B and graph in E), while they also opened up new holes in the bilayer. The adsorbed layer in the defects in Figure 6B is roughly 1.5 $\pm$ 0.2 nm (the difference between the blue and black height scan lines),

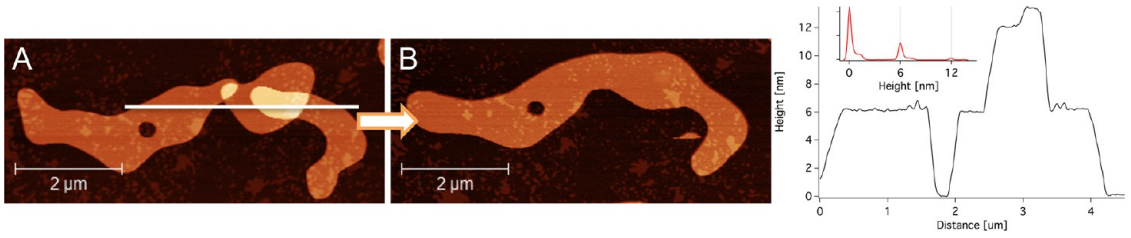

Figure 7. Soft, flexible redeposited patches grew in size by sliding below/above one another, initially forming stacked layers (A), which were then able to coalesce into larger patches (B). The graph shows a height profile corresponding to the white line in A. Inset: Height distribution function of A showing the repeat distance of 6.0 ± 0.2 nm for the stacked patches and a repeated shoulder for each peak, corresponding to the reflection of the topology created by the dendrimers, which can be seen in all levels.

consistent with a dendrimer monolayer adsorbed to clean mica (Figure 3B).

In Figure 5C and Figure 6C (scanning from top to bottom), the dendrimer layer was still present in the defects, but as the scanning continued, all defects were gradually filled up from the edges. The depth of all defects decreased to a mere 1.5 nm as seen from Figure 6D and corresponding height profile in E. With time, both preexistent and newly formed defects expanded in star-like, channel patterns leaving behind only small parts of the original membrane. At the same time, loosely bound islands (white arrow in Figure 5D) began to appear on top of the membrane. This material—coming off the surface—developed into large, flat patches (Figure 5E) having a thickness of 6.0 ± 0.2 nm (see graph in Figure 7). The patches were mobile and able to rotate (Figure 5F) and slide (Figure 5G) between scan lines without perturbing the outline of the structures beneath. These patches followed exactly the topology of the underlying pattern created by the initial dendrimer interaction (compare Figure 5E–H). Hence, we interpret the elevations seen on the outer edges of the floating islands as reflections of the topological arrangement underneath. Furthermore, the patches were able to slide beneath or above one another, creating stacked layers, and then to coalescence into larger islands, as illustrated in Figure 7. The series of images in Figure 5 (and Figure 6) were taken with a lower dendrimer concentration (1 μM) in order to slow down the processes enough to see the different steps of interaction. For 6 μM, a similar overall mechanism was observed, but the speed of the transformation did not allow for resolving the very initial stages of events (see Supporting Information Figure S3 for images with 6 μM concentration).

AFM Imaging of Interaction with Mixed POPC–DPPC Bilayer. When the nominal composition of DPPC was decreased to 80 mol % due to 20 mol % POPC addition, the bilayer displayed gel-phase domains enriched in DPPC coexisting with a fluid phase enriched in POPC (the phase height difference was 1.0 ± 0.2 nm). The difference in the physical state and morphology of the lipid bilayer appeared to have great impact on the outcome of the dendrimer interaction. A time-lapse series of images showing the continuous exposure of an intact bilayer to 6 μM dendrimer solution is presented in Figure 8A–F. The images showed that the dendrimer initially interacted at the edges of the DPPC-rich domains (Figure 8A), followed by a rapid rearrangement of the entire membrane that led to the initial exposure of small areas of the mica substrate (see the vertical height profile shown in Figure 8H (1)). This restructuring of the membrane components was followed by a fast formation of a complex interfacial structural network with ribbon-like protrusions (Figure 8B–F). Imaging while rinsing with PBS (Figure 8G) was performed in order to remove excess dendrimers in the bulk solution, which revealed sharp and well-defined thread-like structures. The reason for this increased resolution upon rinsing is possibly due to the removal of particles attached to the tip that tend to broaden the surface features, but material desorption from the membrane cannot be excluded. It was clear from height profiles (Figure 8H (2)) that the lower part of the image (indicated by a white arrow in Figure 8G) did not correspond to the underlying mica surface, but instead to a layer with a thickness on the order of that of a bilayer.

The layer thickness could be extracted from a height distribution function (see Supporting Information Figure S4), which confirmed a peak at 5.9 ± 0.3 nm similar to the thickness of a DPPC bilayer (see Supporting Information Figure S2), followed by a broad peak centered around 16 nm that corresponds to the mean height of the thread-like structures. This suggests a redistribution of the membrane components so that while a bilayer structure remained underneath, the thread-like protrusions on top were formed by a considerable amount of dendrimers and lipids. At this stage, defects began to appear close to and around the edges of the thread-like structures, indicating that the transformation was not complete.

After 1 day of equilibration, the thread-like structures were still present but pre-existing defects expanded overnight and the system had undergone a further transformation revealing small spherical aggregates at the edges of the former bilayer

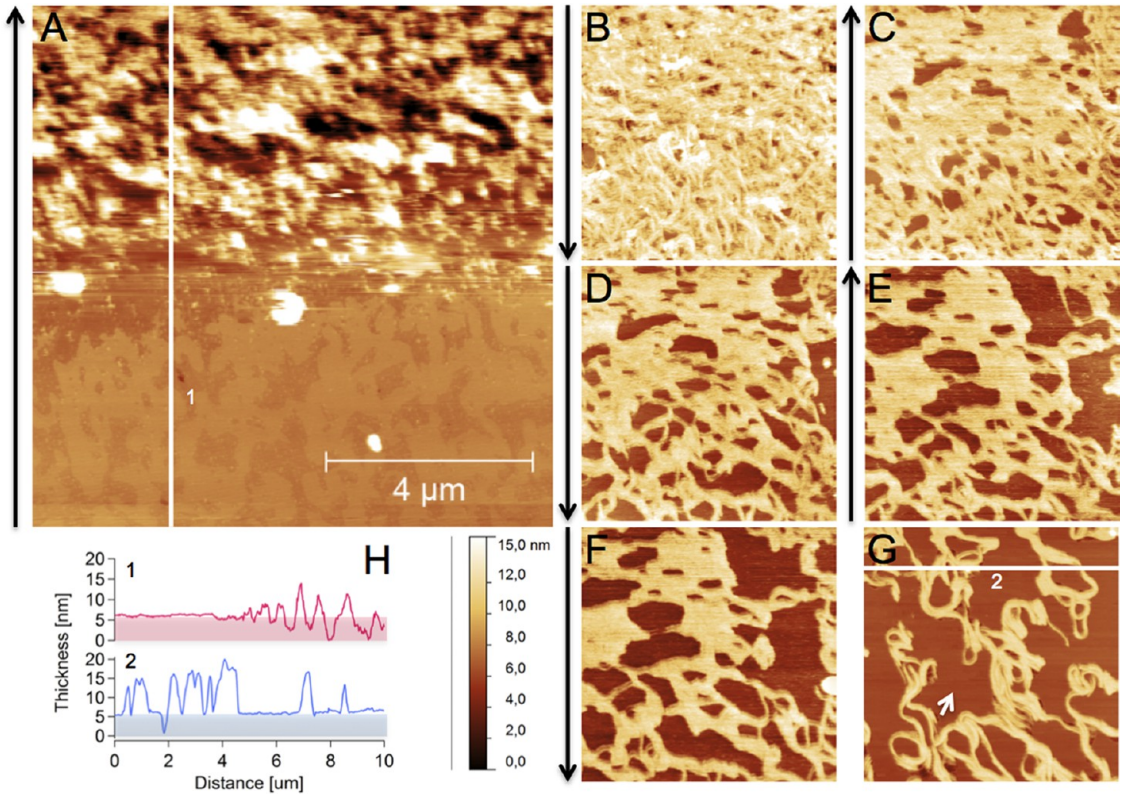

Figure 8. (A–F) Time-lapse series of AFM images showing the encounter of dendrimers on a phase-separated membrane, formation of a network, segregation, and thread-like structures evolving. The scale bar applies to all images, and black arrows indicate the scan direction. (G) Image captured during rinsing with PBS. (H) Height profiles along the line in A(1) and G(2). (1) Shows a complete restructuring of the bilayer components at the onset of interaction, while the depression in (2) shows that the resulting layer has the thickness of a membrane (transparent boxes in H are models of intact bilayers).

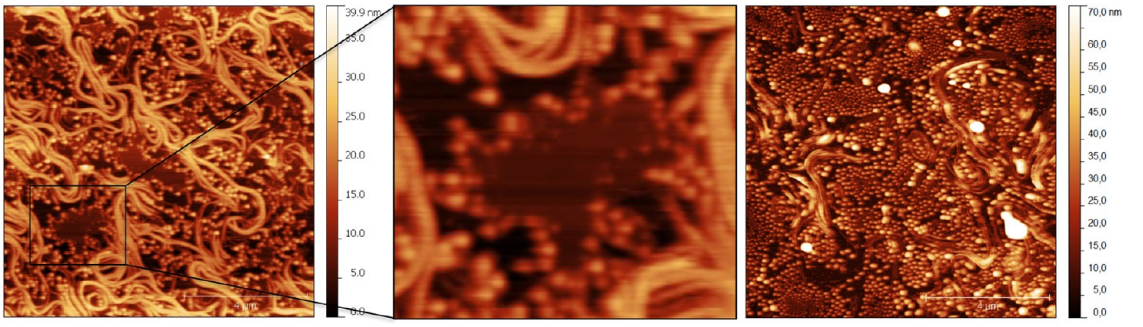

Figure 9. (A) AFM image of the morphological changes observed the day after dendrimer exposure to a phase-separated membrane. The thread-like network was still present, but the layer had partly solubilized over time *via* micellization from the edges of the defects already observed on day 1 and highlighted in Figure 8G,H. (B) Zoom of the boxed area of A. (C) Image of an analogous but different experiment, where all patches have completely transformed into spherical micelle-like structures on day 2.

(compare Figure 8G to Figure 9A). Since areas of the mica surface became exposed, the lipid bilayer appeared partially solubilized by the prolonged incubation (Figure 9A,B). Figure 9C gives an image of a replicate experiment where most of the bilayer had transformed completely into such spherical aggregates. A small area of this image was subsequently subjected to a very high scanning force that allowed for complete removal of the spherical objects from the surface (Supporting Information Figure S5).

In contrast to the slow time-dependent morphological changes seen for the phase-separated membrane, the pure DPPC membrane did not develop thread-like or spherical structures or in any other way change appearance after the main interactions regardless of the dendrimer concentration used (1 or 6 μM) even after 24 h of equilibration time (Figure 5H). Therefore, it is obvious that the mechanisms of action differed significantly with membrane fluidity and the presence of domains.

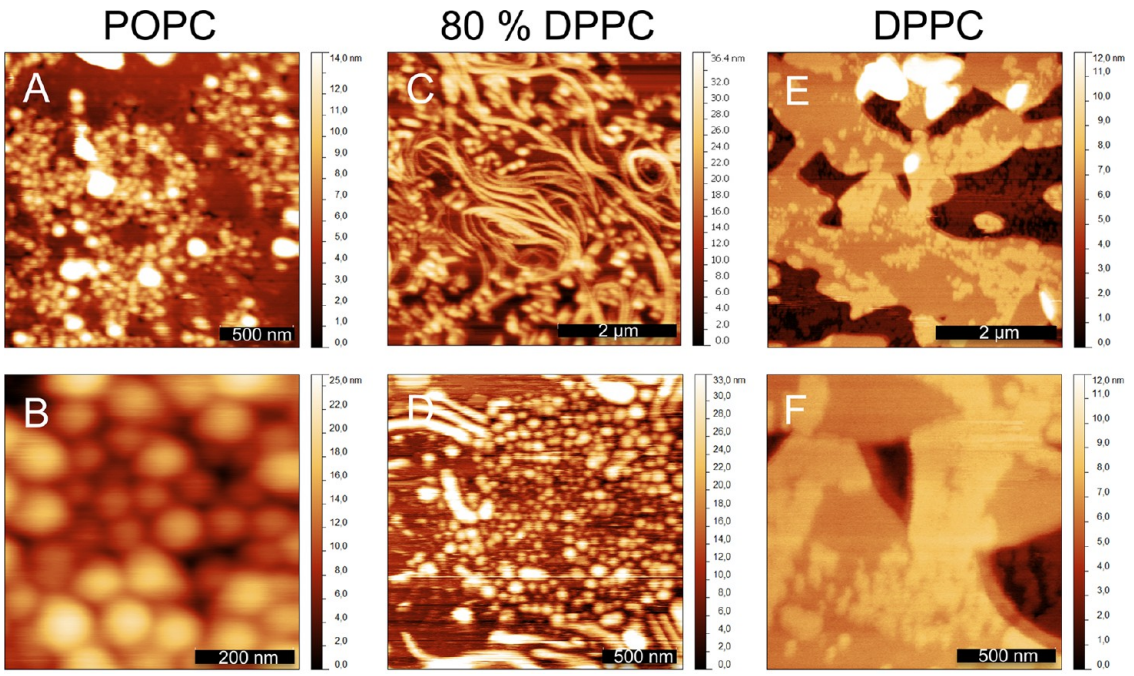

Figure 10. AFM close-ups of (A,B) spherical aggregates formed after interaction with 6 μM BALY and POPC. (C,D) Spherical aggregates and elongated ribbon-like structures formed after interaction between 6 μM BALY and 80 mol % DPPC. These images are from two different experiments. (E,F) Redeposited, flexible patches that follow the topology of the underlying surface morphology after interaction between 6 μM BALY and DPPC. Note the different length and color scales.

AFM Imaging of Interaction with a Fluid POPC Membrane. Dendrimer interaction with a fluid-phase POPC membrane revealed a very different behavior as compared to the gel-phase DPPC membrane, and no signs of local depressions or floating bilayers were seen for a dendrimer concentration of 1 or 6 μM. Instead, discrete spherical aggregates formed through a fast interaction with POPC. High-resolution images of the spherical objects found in POPC can be found in Figure 10A,B together with images resolving the different structures developed in DPPC and the mixed membrane. The spherical aggregates were similar in shape and appearance to those formed in the mixed membrane after one night incubation time. Imaging with dendrimer concentrations as low as 0.1 μM was carried out in order to follow the interaction more closely, but the softness of the fluid membrane during the very initial encounter of the dendrimer did not allow for following those early stages in detail. Since the elongated thread-like tubules were never observed for the single-phase fluid POPC or gel-phase DPPC membranes, they must be a consequence of the mixing of those lipids. These experiments show that there is a requirement for unsaturated PC in order for the dendrimers to induce structures with positive interfacial curvature since thread-like or spherical aggregates were never seen in experiments containing DPPC alone.

DISCUSSION

Processes taking place at biological interfaces are highly dynamic, and it is thus exceedingly important to capture the very initial steps of interaction. Our AFM setup controlled by a slow gravity feed allowed us to follow the initial steps as well as the slower time-dependent interactions under continuous flow of dendrimer solution. To our knowledge, real-time *in situ* nanoparticle interactions have not previously been reported using AFM imaging under constant flow conditions. Previously, we have shown using QCM-D that dendrimer–membrane interactions were dependent on the flow rate, in a way that a full pump stop led to an automatic arrest in the adsorption and layer rearrangement processes taking place.[31] Therefore, continuous flow imaging is preferred for assessing the actual interfacial processes occurring over time and to capture interaction steps that would normally occur within the time it takes to equilibrate the instrument after sample introduction and tip engagement. Upon imaging under continuous flow, it was possible to identify each of the different steps of dendrimer–membrane interaction in a reproducible manner.

The results reported for DPPC in this paper bear resemblance to the membrane thinning actions that Mecke *et al.*[32] reported for antimicrobial peptide MSI-78 with 1,2-dimyristoyl-*sn*-glycero-3-phosphocholine (DMPC). In that case, the interaction also led to areas of locally decreased bilayer thickness, although a significant difference between these two studies was the lipid-phase state. In our experiments, DPPC was in a gel phase, while DMPC was in a fluid state under the experimental conditions used by Mecke *et al.* (28 °C). Since experiments with MSI-78 were not conducted on

gel-phase bilayers, it is not known whether the thinning effect of this linear peptide would occur in a gel-phase membrane, as well. Janshoff *et al.*[33] showed that an amphipathic helix-forming peptide involved in membrane permeabilization inserted in fluid-phase DPPC, but caused local areas of 1.5 ± 0.2 nm depressions only after cooling below the transition temperature. In both of these cases, the depressions formed were similar in depth to our results for BALY on DPPC (see Figures 5−7), but the authors did not observe redeposition of floating "bilayer" patches as in our case. However, lipid sedimentation processes for gel-phase DPPC membranes were previously observed by AFM upon exposure to *n*-octyl β-D-glucopyranoside (OG) above its critical micelle concentration.[34] OG is a widely used detergent for membrane reconstitution procedures, and the molecules caused the gel-phase membrane to first desorb from the surface and subsequently reconstitute on the surface as a planar lipid−surfactant membrane. Since our dendrimer possesses amphiphilic properties (surfactant-like) and caused similar redeposition of flat patches for gel-phase lipids as OG, these processes may be of similar origin. The BALY dendrimer did not form spherical aggregates in the gel-phase membrane while it formed rod-like or spherical aggregates when POPC was present. This may be due to the more constrained DPPC tails as compared to the flexible POPC tails (Figures 8−10). For DPPC, BALY molecules adsorbed on the lipid surface and enabled bridging between flat, dendrimer-stabilized, disk-like patches and the underlying layer. The four long amphiphilic arms of the dendrimer could possibly mediate this lubrication effect, resulting in loosely bound sliding or floating islands. For POPC, complete dendrimer−lipid mixing may occur instead.

Another antimicrobial helix-forming peptide, Melittin, has been shown to also interact *via* different mechanisms depending on the lipid-phase state. AFM images captured by Oliynyk *et al.*[35] showed that Melittin premixed with gel-phase DPPC produced flat, perforated patches (and even small areas of redeposited bilayer sheets). For a premixed sample of fluid 1,2-dilauroyl-*sn*-glycero-3-phosphocholine (DLPC), small spherical complexes were observed similar to the ones formed by POPC−BALY. Instead, in gel-phase DPPC, Melittin gave rise to full-depth pores that were surrounded by ridges with a step height similar to the depressions reported here, suggesting that the peptide induced a phase change at these edges. The differences in the AFM results between these two studies could very well be a consequence of the methods used for sample preparation since deposition of a premixed peptide/lipid solution to a surface may give rise to a different layer structure and does not show the different stages of interaction that we resolve here. However, the study suggests that the linear antimicrobial peptide, Melittin, may have some similar ways of interacting as our branched peptide dendrimer BALY.

Bilayer disruption and solubilization of fluid-phase egg PC (predominantly POPC) by amphiphilic, α-helix-forming peptide p25 was also observed using AFM by Rigby-Singleton *et al.*[36] They found that the peptide caused formation of sphere-like features in the areas between mica and lipid bilayer edges, bearing resemblance to the ones reported for BALY on POPC-containing bilayers. They suggested a "budding mechanism" where the peptide induces positive curvature of the upper membrane leaflet and thus a decrease in the lipid packing parameter, leading to highly curved mixed spherical aggregates. The images showed defects growing from the edges out, expanding in a channeling pattern and leaving back surface-active spherical aggregates on the mica. Thus, this peptide seems to solubilize the fluid lipid membrane *via* mixed dendrimer−lipid aggregates in a similar way as our dendrimer does. Mecke *et al.*[37,38] proposed that G7 PAMAM dendrimers can form lipid−dendrimer vesicles (dendrisomes) and remove bilayer patches due to a high number of stabilizing bonds between the dendrimer surface groups and the lipid molecules, while the much smaller G3 PAMAM dendrimers have too few stabilizing bonds to form a lipid−dendrimer vesicle and thus cannot remove lipids from a bilayer *via* this mechanism. However, Parimi *et al.* have observed a (nonlinear) concentration-dependent lipid removal of fluid DMPC bilayers even for G2 and G4 PAMAM dendrimers,[39] which implies an alternative mechanism at very low generations. The vesicular solubilization mechanism proposed by Rigby-Singleton *et al.*[36] was suggested to involve a lipid−peptide matrix surrounding the outer leaflet, while the inner leaflet remained peptide-free due to packing restrictions. As in our experiments, neither the composition of these complexes nor the nature of the aggregates (vesicular *versus* micellar) can be extracted from AFM studies. However, due to both bilayer curvature restrictions and to a limited number of stabilizing bonds, it is not likely that a bilayer patch wraps around a single dendrimer molecule to form a dendrimer-enclosed lipid vesicle. For these vesicles to form, the core would have to be constituted by larger dendrimer aggregates. A model of such a collective action by small dendrimers at high concentrations has been supported by isothermal thermal calorimetry (ITC) stoichiometric data by Kelly *et al.*[40] It is also likely that the spherical structures (Figures 9 and 10) are micelle-like structures that remain surface-active. A similar mechanism was previously proposed[41] as an alternative to the lipid−dendrimer vesicle formation based on AFM images of drug surfactant−dendrimer complexes.[42] It seems clear, however, that the mechanism of BALY dendrimers is different from PAMAM dendrimers in general.

For the latter, interaction usually leads to lipid removal and exposes regions of lipid-free surface, while BALY—lipid aggregates adsorbed and remained attached to the membrane surface by a mechanism that closer resembles peptide and surfactant interaction with lipid membranes.

The BALY dendrimer is one out of a diverse library of peptide dendrimers showing different activity, toxicity and selectivity depending on their level of branching and the types of functional groups that they present.[43,44] It has previously been reported that significant activity variations can be expected for such differing topologies.[16,45] Indeed, preliminary QCM-D and AFM experiments with other dendrimers from this library performed in our group suggest that these chemical variations have a profound effect on the interaction mechanisms. Therefore, we do not believe that the interactions discussed in this paper represent a general mechanism for peptide-based dendrimers but rather a structure-dependent mechanism, which could share similarities with various other types of nanoparticles. Due to the amphiphilic character of the dendrimers and the antimicrobial profile resembling that of AMPs, mechanistic aspects of their biological activity is expected to show analogy to the interaction mechanisms of linear amphiphilic peptides rather than to polycationic PAMAM, PPI carbosilane, *etc.* dendrimers.

From QCM-D and AFM, it is not possible to determine how the dendrimers and lipids redistribute upon interaction and whether dendrimers cause interdigitation or thinning in the gel-phase membranes. In order to properly establish the nature of these complex mechanisms, molecular dynamics simulations and neutron reflection experiments are planned. So far, we have investigated the effect of membrane fluidity, and we are at the moment extending our studies to understand the role of membrane surface charge density and specific effects of the lipid headgroup. For the latter, we are currently developing methods to form supported lipid bilayers from lipids extracted from bacterial strains of interest. It has been proposed that the dense peptidoglycan layer of Gram-positive bacteria acts solely as a sieve, permitting only small molecules of 3 kDa or less to penetrate and interact with the plasma membrane.[46] Based on this view, our BALY dendrimer will be in the size range of penetrating peptides (2 kDa), and thus a bacterial lipid membrane mimic containing charged lipids should suffice as a simple model to describe the mechanism of interaction with bacterial cell surfaces.

CONCLUSION

We have confirmed that the amphiphilic character of our dendrimer allowed it to partition into the water—lipid interface, causing complete lipid rearrangement, and to induce phase change or increased lipid curvature depending on the lipid-phase state. The mechanism of interaction between the dendrimer and lipid bilayers was thus found to be dependent on the lipid phase and consistent with a requirement for unsaturation for lipid—dendrimer micelle-like complex formation and solubilization of the lipid membrane in a detergent-like manner. A purely saturated bilayer in the gel phase was instead disrupted *via* expansion of dendrimer-induced local depressions in the membrane and redeposition of membrane patches similar to detergent membrane reconstitution, probably due to dendrimer adsorption and partial penetration into the lipid bilayer.

Our observations of time-dependent network formation and slow solubilization of phase-separated lipid bilayers are rather different from previous reports on more widely studied PAMAM dendrimers and, to our knowledge, unlike any peptide or dendrimer interaction reported before. BALY mixes with lipids in a fluidity-dependent manner and seems to share some similarities with antimicrobial peptides and surfactants. Our optimized experimental setup designed for a concentration range covering the minimal inhibitory concentration of the dendrimer sheds light on a molecular mechanism of antimicrobial activity, which in general is hard to obtain.

MATERIALS AND METHODS

POPC and DPPC were purchased from Avanti Polar Lipids, Inc. (Alabaster, AL) and used without further purification. L-Lysine was purchased from IRIS Biotech GMBH. *N*,*N*′-Dicyclohexylcarbodiimide (DCC), hydroxybenzotriazole (HOBt), *N*-hydroxysuccinimide (HOSu), chloroform, *N*,*N*-dimethylformamide (DMF), methyl alcohol (MeOH), ethylenediamine, and sodium chloride (NaCl) were purchased from Sigma Aldrich Inc. Sodium phosphate monobasic (Na_2HPO_4) and sodium phosphate dibasic (NaH_2PO_4) were purchased from Fluka Analytical. Ultrapure Milli-Q (MQ) water with a resistivity of 18.2 MΩ (Thermo Scientific, Branstead Nanopure 7145) was used for all cleaning procedures, samples, and buffer preparation. Hellmanex 2% (Hellma GmbH & Co., Germany) and absolute ethanol were used for cleaning QCM-D sensor crystals purchased from Q-Sense AB (Västre Frölunda, Sweden).

Dendrimer Solutions. Prior to use, dendrimers were dissolved in small quantities of methanol. For experiments, the dendrimers were diluted into 10 mM phosphate buffered saline (PBS) containing 100 mM NaCl at pH 7.4 to concentrations ranging from 1 to 50 μM. In all experiments, dendrimers were bath-sonicated (Branson 1510, Branson Ultrasonics Corporation, USA) prior to introduction to the bilayer to eliminate kinetically trapped self-aggregates formed in solution.

Small Unilamellar Vesicle (SUV) Preparation. Lipids dissolved in chloroform were dried under a soft stream of nitrogen onto the walls of clean glass vials. The films were left in vacuum overnight in order to remove any remaining organic solvent and stored at −18 °C until use. Lipid films were resuspended in PBS to a concentration of 0.5−1 mg/mL and were left to hydrate for a minimum 1 h at a temperature at least 10 °C above the highest melting temperature of the lipids in the mixture (DPPC, T_m = 42 °C;

POPC, $T_m = -4$ °C). SUVs were prepared by tip sonication of the suspensions until clarity. Sonication was carried out on a 50% duty cycle (5 s on followed by 5 s off) in order to reduce the heat produced.

Dissipation-Enhanced Quartz Crystal Microbalance. Experiments were performed with the Q-SENSE E4 system (Biolin Scientific AB, Sweden). The quartz sensor crystals used were coated with 50 nm silicon dioxide, purchased from Q-Sense. For cleaning, O-rings and the sensor surfaces were placed in 2% Hellmanex for 10 min followed by thorough rinsing in absolute ethanol and ultrapure water. They were then dried in a stream of nitrogen, and the surfaces were subsequently oxidized in a UV-ozone chamber (BioForce Nanosciences, Inc., Ames, IA) for 10 min in order to remove any organic contamination. Before performing any measurements, the instrument was equilibrated at 25 °C until a stable baseline in water was recorded.

The isotherm of BALY adsorption to clean mica was obtained using dendrimer solutions of concentrations ranging from 1 to 50 μM. For all concentrations, the adsorption was carried out on a clean surface as follows: 1 h adsorption under a constant flow of 100 μL/min, 1 h equilibration, and 1 h rinsing with PBS at 100 μL/min.

Lipids were pumped into the sample cells at a concentration of 100 μg/mL, at 25 °C for 0 mol % DPPC, and at 50 °C for mixtures containing DPPC. After successful supported bilayer formation, the membranes were rinsed with PBS and cooled to 25 °C before addition of dendrimers.

Atomic Force Microscopy. Measurements were carried out on a Nanoscope IV multimode AFM (Veeco Instruments Inc.). Images were generated in the PeakForce quantitative mechanical property mapping (QNM) mode with a silicon oxide tip (Olympus microcantilever OTR8 PS-W) having a spring constant of 0.15 N/m and a radius of curvature of <20 nm. PeakForce tapping mode is different from contact and traditional tapping mode since it allows for precisely controlling the imaging force in order to keep indentations small, thus enabling nondestructive and high-resolution imaging. This mode is ideal for imaging of soft matter in liquid environments at high resolution. A liquid flow cell (glass probe holder, MTFML, Bruker Corporation) was used to scan the surfaces in a liquid environment and to exchange solution *in situ*. The setup was optimized for real-time continuous flow imaging where the solution constantly exchanges *via* a slow gravity feed. The slow feed was produced by careful control of the height difference between the inlet and the outlet and allowed for a gentle flow through the cell without causing disturbance around the cantilever. In this way, a (nonlinear) flow was obtained and optimized to vary between 40 and 50 μL/min (minimum flow rate) in order to increase the spatial and time resolution.

First, a freshly cleaved mica surface was imaged in ultrapure water in order to ensure a clean and smooth surface (rms <500 pm) prior to bilayer measurements. Small unilamellar vesicles were introduced into the AFM flow cell, and bilayer formation and vesicle attachment were imaged. For hot depositions, the cell was preheated with pure water (80 °C) just prior to introduction of a SUV solution heated to 55 °C. The lipids were incubated in the AFM for at least 30 min and imaged to secure high coverage before rinsing the membrane with water. Before introducing dendrimers, the membranes were rinsed in excess PBS, pH 7.4. The dendrimer solution was introduced to the membrane, and the flow was maintained while imaging for at least 90 min. In this way, new dendrimers were continuously brought to the interface during scanning. Then the membrane was rinsed with PBS while imaging. The membranes were left overnight and imaged again in order to observe potential kinetically slow processes happening on larger time scales. Advantages of imaging under flow conditions include that (1) no equilibration time is needed between injections, thus imaging is performed with no delay, and (2) no shift in the imaged area is induced by retracting and engaging the tip between injections (although a slight shift can occur during imaging). All images were recorded at a resolution of 512 × 512 pixels and with a scan rate of 1 Hz. The z-set point and differential gains were manually optimized during each scan. Images were analyzed and processed in the Gwyddion 2.22 software.

Microbiology and Hemotoxicity. Bacteria *Staphylococcus aureus* spp. *aureus* ATCC 25923, *Pseudomonas aeruginosa* ATCC 27853, *Escherichia coli* ATCC 25922, and *Staphylococcus aureus* spp. *aureus* ATCC 43300 were cultivated on tryptone/soy agar (TSA; Oxoid). Mueller–Hinton broth (Oxoid) was supplemented with cations: 12.5 mg Mg^{2+}/L and 25 mg Ca^{2+}/L. The pH of the medium after sterilization was between 7.2 and 7.4 [cation-adjusted Mueller–Hinton broth (CAMHB)].

Broth microdilution susceptibility test was performed as described in Committee Laboratory Standards (CLSI) reference method M07-A8.[47] Briefly, a series of the two-fold dendrimer dilutions in DMSO and two-fold polymyxin B and penicillin G dilutions in CAMHB were diluted 1:94 with CAMHB. Then, 95 μL aliquots were dispensed into microdilution sterile plates (Mar-Four). Then, 5 μL of bacteria inoculum containing 5×10^4 CFU/mL was added. The final concentration of dendrimer ranged from 64 to 2 μg/mL, polymyxin B and penicillin G from 8 to 0.15 μg/mL, all in two-fold dilution steps. The plates were incubated at 35 °C and read after 18 or 24 h depending on bacterial strain. MICs, measured in triplicate, were defined as the lowest drug concentration that reduced growth by 100%. Dendrimer-induced hemolysis was measured using serum-free human red blood cells obtained from the Institute of Hematology and Transfusion Medicine in Warsaw, suspended in PBS, pH 7.4. Prepared suspension of 1% hematocrit was incubated with serial concentration of dendrimers for 30 min at 23 °C. After centrifugation (1000 rpm, 5 min), the absorbance of the supernatant was measured at 540 nm (Jasco 630, Japan). A value of 100% hemolysis was determined by incubation of erythrocytes with double-distilled water (30 min at 23 °C). In a control experiment, cells were incubated in buffer without peptide, and absorbance at 540 nm was used as a blank.

Conflict of Interest: The authors declare no competing financial interest.

Acknowledgment. The authors wish to thank A. Åkesson for help with QCM-D measurements. T.K.L. and M.C. gratefully acknowledge financial support from the Center for Synthetic Biology at Copenhagen University funded by the UNIK research initiative of the Danish Ministry of Science, Technology and Innovation, and the European Spallation Source in Lund, Sweden. P.Z. thanks the Ministry of Science and Higher Education of Poland (Grant N204 239436) for covering the cost of synthesis and electron microscopy studies.

Supporting Information Available: MICs of BALY toward various bacterial strains and the synthetic route to BALY including MSLR, ESI, ^{1}H NMR, and ^{13}C NMR data. QCM-D raw data for BALY interaction with POPC, 80 mol % DPPC, and DPPC. AFM image and height distribution of a DPPC bilayer prior to interaction with BALY. AFM images and height profile of 6 μM BALY interacting with DPPC. Height distribution function of the AFM image in Figure 8G in the main text. AFM image and height profile of 80 mol % DPPC subjected to high scanning force to remove objects formed after 1 day of incubation. This material is available free of charge *via* the Internet at http://pubs.acs.org.

REFERENCES AND NOTES

1. Cars, O.; Hedin, A.; Heddini, A. Drug Resistance Updates: The Global Need for Effective Antibiotics—Moving Towards Concerted Action. *Drug Resist. Update* **2011**, 68–69.
2. Rangel, J. M.; Sparling, P. H.; Crowe, C.; Griffin, P. M.; Swerdlow, D. L. Epidemiology of *Escherichia coli* O157:H7 Outbreaks, United States, 1982–2002. *Emerg. Infect. Dis.* **2005**, *11*, 603–609.
3. Tenover, F. C. Mechanisms of Antimicrobial Resistance in Bacteria. *Am. J. Med.* **2006**, *119*, S3–S10.
4. Walsh, C. Molecular Mechanisms That Confer Antibacterial Drug Resistance. *Nature* **2000**, *406*, 775–781.
5. Zasloff, M. Antimicrobial Peptides of Multicellular Organisms. *Nature* **2002**, *415*, 389–395.
6. Boman, H. G. Peptide Antibiotics and Their Role in Innate Immunity. *Annu. Rev. Immunol.* **1995**, *13*, 61–92.
7. Fernebro, J. Fighting Bacterial Infections: Future Treatment Options. *Drug Resist. Update* **2011**, *14*, 125–139.

8. Tam, J. P.; Lu, Y. A.; Yang, J. L. Antimicrobial Dendrimeric Peptides. *Eur. J. Biochem.* **2002**, *269*, 923–932.
9. Brogden, K. A. Antimicrobial Peptides: Pore Formers or Metabolic Inhibitors in Bacteria? *Nat. Rev. Microbiol.* **2005**, *3*, 238–250.
10. Reddy, K. V. R.; Yedery, R. D.; Aranha, C. Antimicrobial Peptides: Premises and Promises. *Int. J. Antimicrob. Agents* **2004**, *24*, 536–547.
11. Calabretta, M. K.; Kumar, A.; McDermott, A. M.; Cai, C. Antibacterial Activities of Poly(amidoamine) Dendrimers Terminated with Amino and Poly(ethylene glycol) Groups. *Biomacromolecules* **2007**, *8*, 1807–1811.
12. Chen, C. Z.; Beck-Tan, N. C.; Dhurjati, P.; van Dyk, T. K.; LaRossa, R. A.; Cooper, S. L. Quaternary Ammonium Functionalized Poly(propylene imine) Dendrimers as Effective Antimicrobials: Structure−Activity Studies. *Biomacromolecules* **2000**, *1*, 473–480.
13. Rasines, B.; Hernández-Ros, J. M.; de las Cuevas, N.; Copa-Patiño, J. L.; Soliveri, J.; Muñoz-Fernández, M. A.; Gómez, R.; de la Mata, F. J. Water-Stable Ammonium-Terminated Carbosilane Dendrimers as Efficient Antibacterial Agents. *Dalton Trans.* **2009**, 8704–8713.
14. Ortega, P.; Cobaleda, B. M.; Hernández-Ros, J. M.; Fuentes-Paniagua, E.; Sánchez-Nieves, J.; Tarazona, M. P.; Copa-Patiño, J. L.; Soliveri, J.; de la Mata, F. J.; Gómez, R. Hyperbranched Polymers *versus* Dendrimers Containing a Carbosilane Framework and Terminal Ammonium Groups as Antimicrobial Agents. *Org. Biomol. Chem.* **2011**, *9*, 5238–5248.
15. Meyers, S. R.; Juhn, F. S.; Griset, A. P.; Luman, N. R.; Grinstaff, M. W. Anionic Amphiphilic Dendrimers as Antibacterial Agents. *J. Am. Chem. Soc.* **2008**, *130*, 14444–14445.
16. Stach, M.; Maillard, N.; Kadam, R. U.; Kalbermatter, D.; Meury, M.; Page, M. G. P.; Fotiadis, D.; Darbre, T.; Reymond, J.-L. Membrane Disrupting Antimicrobial Peptide Dendrimers with Multiple Amino Termini. *MedChemComm* **2012**, *3*, 86–89.
17. Ravi, H. K.; Stach, M.; Soares, T. A.; Darbre, T.; Reymond, J.-L.; Cascella, M. Electrostatics and Flexibility Drive Membrane Recognition and Early Penetration by the Antimicrobial Peptide Dendrimer Bh1. *Chem. Commun.* **2013**, *49*, 8821–8823.
18. Janiszewska, J.; Urbanczyk-Lipkowska, Z. Amphiphilic Dendrimeric Peptides as Model Non-sequential Pharmacophores with Antimicrobial Properties. *J. Mol. Microbiol. Biotechnol.* **2007**, *13*, 220–225.
19. Klajnert, B.; Janiszewska, J.; Urbanczyk-Lipkowska, Z.; Bryszewska, M.; Shcharbin, D.; Labieniec, M. Biological Properties of Low Molecular Mass Peptide Dendrimers. *Int. J. Pharm.* **2006**, *309*, 208–217.
20. Janiszewska, J.; Swieton, J.; Lipkowski, A. W.; Urbanczyk-Lipkowska, Z. Low Molecular Mass Peptide Dendrimers That Express Antimicrobial Properties. *Bioorg. Med. Chem. Lett.* **2003**, *13*, 3711–3713.
21. Giuliani, A.; Pirri, G.; Nicoletto, S. F. Antimicrobial Peptides: An Overview of a Promising Class of Therapeutics. *Cent. Eur. J. Biol.* **2007**, *2*, 1–33.
22. Stromstedt, A. A.; Ringstad, L.; Schmidtchen, A.; Malmsten, M. Interaction between Amphiphilic Peptides and Phospholipid Membranes. *Curr. Opin. Colloid Interface Sci.* **2010**, *15*, 467–478.
23. Melo, M. N.; Ferre, R.; Castanho, M. A. Antimicrobial Peptides: Linking Partition, Activity and High Membrane-Bound Concentrations. *Nat. Rev. Microbiol.* **2009**, *7*, 245–250.
24. Castonguay, A.; Ladd, E.; van de Ven, T. G. M.; Kakkar, A. Dendrimers as Bactericides. *New J. Chem.* **2012**, *36*, 199–204.
25. Shoemaker, S. D.; Vanderlick, T. K. Material Studies of Lipid Vesicles in the L-α and L-α-Gel Coexistence Regimes. *Biophys. J.* **2003**, *84*, 998–1009.
26. Curatolo, W.; Sears, B.; Neuringer, L. J. A Calorimetry and Deuterium NMR-Study of Mixed Model Membranes of 1-Palmitoyl-2-oleylphosphatidylcholine and Saturated Phosphatidylcholines. *Biochim. Biophys. Acta* **1985**, *817*, 261–270.
27. Åkesson, A.; Lind, T.; Ehrlich, N.; Stamou, D.; Wacklin, H. P.; Cárdenas, M. Composition and Structure of Mixed Phospholipid Supported Bilayers Formed by POPC and DPPC. *Soft Matter* **2012**, *8*, 5658–5665.
28. Rodahl, M.; Höök, F.; Krozer, A.; Brzezinski, P.; Kasemo, B. Quartz Crystal Microbalance Setup for Frequency and Q-Factor Measurements in Gaseous and Liquid Environments. *Rev. Sci. Instrum.* **1995**, *66*, 3924–3930.
29. Cho, N.-J.; Frank, C. W.; Kasemo, B.; Höök, F. Quartz Crystal Microbalance with Dissipation Monitoring of Supported Lipid Bilayers on Various Substrates. *Nat. Protoc.* **2010**, *5*, 1096–1106.
30. Richter, R. P.; Brisson, A. R. Following the Formation of Supported Lipid Bilayers on Mica: A Study Combining AFM, QCM-D, and Ellipsometry. *Biophys. J.* **2005**, *88*, 3422–3433.
31. Akesson, A.; Lind, T. K.; Barker, R.; Hughes, A.; Cardenas, M. Unraveling Dendrimer Translocation across Cell Membrane Mimics. *Langmuir* **2012**, *28*, 13025–13033.
32. Mecke, A.; Lee, D.-K.; Ramamoorthy, A.; Orr, B. G.; Holl, M. M. B. Membrane Thinning Due to Antimicrobial Peptide Binding: An Atomic Force Microscopy Study of MSI-78 in Lipid Bilayers. *Biophys. J.* **2005**, *89*, 4043–4050.
33. Janshoff, A.; Bong, D. T.; Steinem, C.; Johnson, J. E.; Ghadiri, M. R. An Animal Virus-Derived Peptide Switches Membrane Morphology: Possible Relevance to Nodaviral Transfection Processes. *Biochemistry* **1999**, *38*, 5328–5336.
34. Morandat, S.; El Kirat, K. Solubilization of Supported Lipid Membranes by Octyl Glucoside Observed by Time-Lapse Atomic Force Microscopy. *Colloids Surf., B* **2007**, *55*, 179–184.
35. Oliynyk, V.; Kaatze, U.; Heimburg, T. Defect Formation of Lytic Peptides in Lipid Membranes and Their Influence on the Thermodynamic Properties of the Pore Environment. *Biochim. Biophys. Acta* **2007**, *1768*, 236–245.
36. Rigby-Singleton, S. M.; Davies, M. C.; Harris, H.; O'Shea, P.; Allen, S. Visualizing the Solubilization of Supported Lipid Bilayers by an Amphiphilic Peptide. *Langmuir* **2006**, *22*, 6273–6279.
37. Mecke, A.; Uppuluri, S.; Sassanella, T. M.; Lee, D.-K.; Ramamoorthy, A.; Baker, J. R., Jr.; Orr, B. G.; Banaszak Holl, M. M. Direct Observation of Lipid Bilayer Disruption by Poly(amidoamine) Dendrimers. *Chem. Phys. Lipids* **2004**, *132*, 3–14.
38. Mecke, A.; Majoros, I. J.; Patri, A. K.; Baker, J. R.; Banaszak Holl, M. M.; Orr, B. G. Lipid Bilayer Disruption by Polycationic Polymers: The Roles of Size and Chemical Functional Group. *Langmuir* **2005**, *21*, 10348–10354.
39. Parimi, S.; Barnes, T. J.; Prestidge, C. A. Pamam Dendrimer Interactions with Supported Lipid Bilayers: A Kinetic and Mechanistic Investigation. *Langmuir* **2008**, *24*, 13532–13539.
40. Kelly, C. V.; Liroff, M. G.; Triplett, L. D.; Leroueil, P. R.; Mullen, D. G.; Wallace, J. M.; Meshinchi, S.; Baker, J. R.; Orr, B. G.; Holl, M. M. B. Stoichiometry and Structure of Poly(amidoamine) Dendrimer−Lipid Complexes. *ACS Nano* **2009**, *3*, 1886–1896.
41. Smith, P. E. S.; Brender, J. R.; Dürr, U. H. N.; Xu, J.; Mullen, D. G.; Banaszak Holl, M. M.; Ramamoorthy, A. Solid-State NMR Reveals the Hydrophobic-Core Location of Poly(amidoamine) Dendrimers in Biomembranes. *J. Am. Chem. Soc.* **2010**, *132*, 8087–8097.
42. Cheng, Y. Y.; Wu, Q. L.; Li, Y. W.; Hu, J. J.; Xu, T. W. New Insights into the Interactions between Dendrimers and Surfactants: 2. Design of New Drug Formulations Based on Dendrimer−Surfactant Aggregates. *J. Phys. Chem. B* **2009**, *113*, 8339–8346.
43. Polcyn, P.; Jurczak, M.; Rajnisz, A.; Solecka, J.; Urbanczyk-Lipkowska, Z. Design of Antimicrobially Active Small Amphiphilic Peptide Dendrimers. *Molecules* **2009**, *14*, 3881–3905.
44. Janiszewska, J.; Sowinska, M.; Rajnisz, A.; Solecka, J.; Łacka, I.; Milewski, S.; Urbanczyk-Lipkowska, Z. Novel Dendrimeric Lipopeptides with Antifungal Activity. *Bioorg. Med. Chem. Lett.* **2012**, *22*, 1388–1393.

45. Polcyn, P.; Zielinska, P.; Zimnicka, M.; Troć, A.; Kalicki, P.; Solecka, J.; Laskowska, A.; Urbanczyk-Lipkowska, Z. Novel Antimicrobial Peptide Dendrimers with Amphiphilic Surface and Their Interactions with Phospholipids: Insights from Mass Spectrometry. *Molecules* **2013**, *18*, 7120–7144.
46. Lienkamp, K.; Kumar, K. N.; Som, A.; Nusslein, K.; Tew, G. N. "Doubly Selective" Antimicrobial Polymers: How Do They Differentiate between Bacteria? *Chemistry* **2009**, *15*, 11710–11714.
47. CLSI. uM CLSI: 940 West Valley Road, Suite 1400, Wayne, Pennsylvania 19087-1898, USA, **2009**.